Electronic Supplementary Material

31 March, 2020

MS. ID: LC-ART-01-2020-000082

Hybrid Paper and 3D-Printed Microfluidic Device for Electrochemical Detection of Ag Nanoparticle Labels

Charuksha Walgama, Michael P. Nguyen, Lisa M. Boatner, Ian Richards, and Richard M. Crooks

Table of Contents

Fabrication of paper electrodes (*hy*Flow and *no*Flow devices). The *hy*Flow paper electrodes have a T-shaped design (Figure S1). They were fabricated as follows. First, a template was designed using CorelDRAW (Ottawa, ON) and then it was wax printed on sheets of chromatography paper using a Xerox ColorQube 8570DN printer. Each printout yields eight separate electrodes (Figure S2). After printing, the wax was melted through the thickness of the paper by placing it in an oven at 120 ^{0}C for 25 s. Second, the wax-patterned paper was glued onto a sheet of Kodak photo paper using a glue stick, and then the back side of the photo paper was covered with transparent packaging tape. This process creates a rigid, non-wetting backing for the paper electrodes. Third, the paper was cut into eight rectangles, each containing one *hy*Flow paper electrode (Figure S2). Fourth, a stencil pattern of the three electrodes was created using CorelDRAW, and then it was cut into a thin plastic sheet of transparency film using a laser engraving system (Epilog Laser Zing 16). The stencil was aligned over each rectangular paper (wax side up), and the electrodes were screen printed through the stencil using conductive carbon paste. The carbon paste was left to dry in air for 14 h. Finally, the T-shaped *hy*Flow paper electrodes were cut using scissors and the inlets were punched using a hole punch.

   The fabrication of the *no*Flow paper electrode was similar to that of the *hy*Flow paper electrode but the electrochemical analysis was performed as a droplet assay rather than in a flow format. The *no*Flow and *hy*Flow electrodes have the same dimensions, but the *no*Flow lacks the yellow-waxed flow path and the paper sink (Figure S3).
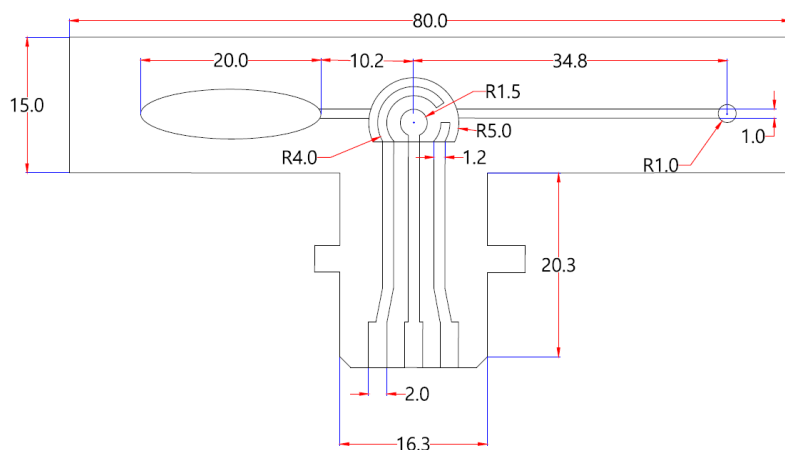
Figure S1. AutoCAD drawing of the *hy*Flow paper electrode (all dimensions are given in mm, R = radius).
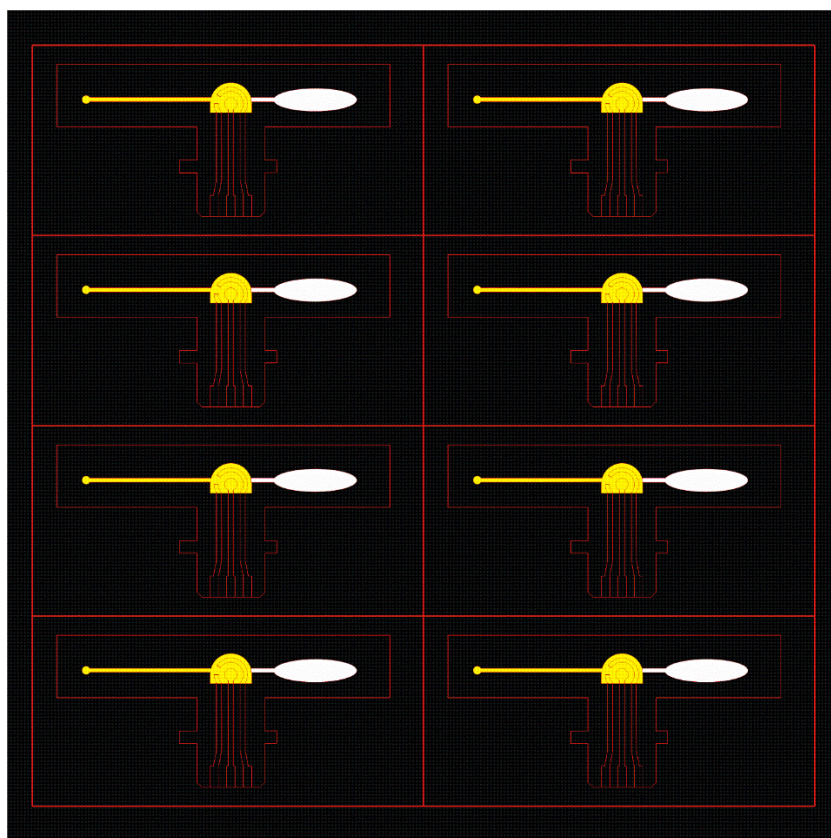

Figure S2. Drawing of the *hy*Flow paper electrode design that is wax printed onto chromatography paper. Each printout yields eight electrode assemblies. The yellow area includes the channel and electrode assembly, and the white area is the wicking pad.
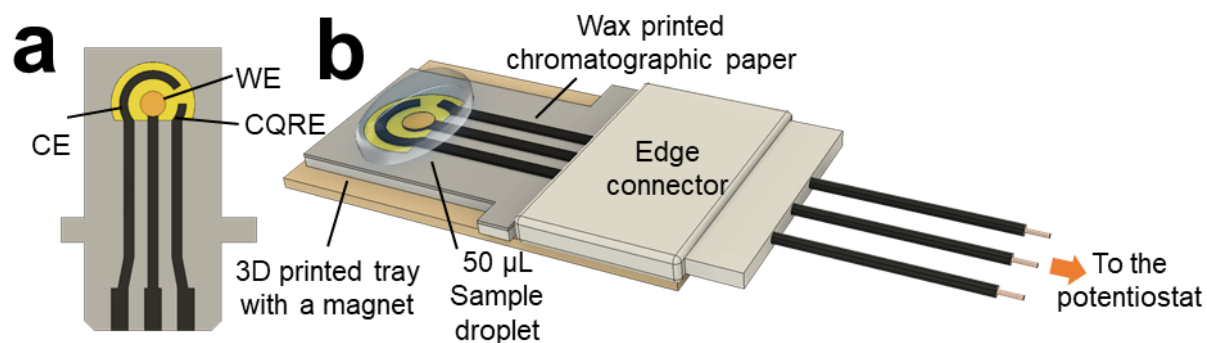
Figure S3. Schematic illustration of the *no*Flow electrode assembly. (a) Schematic representation of the wax printed *no*Flow paper electrode platform with screen printed conductive carbon paste electrodes (CE = carbon counter electrode, WE (C/Au) = carbon working electrode with electrodeposited Au, and CQRE = carbon quasi-reference electrode). (b) The entire *no*Flow assembly. The electrodes are connected to the edge connector to ensure an ohmic contact with the potentiostat. The bottom piece of the edge connector has a 3D-printed plastic extension to align a magnet with the center of the working electrode. The magnet is used to concentrate the MB–AgNP conjugates onto the working electrode.

3D Printing. A computer-aided 3D design was generated using Autodesk Fusion 360 software (San Rafael, CA), and then it was converted to a 3D printer compatible STL file. The parts were printed using a clear resin composed of methacrylic acid esters and a photoinitiator provided by the manufacturer.

   After fabrication, 3D-printed parts (Figure S4) were immediately submerged in an isopropanol bath for 15 min to remove uncured resin, and then the two pieces were dried and further cured in a UV incubator for 2 h. After masking the microfluidic channel and the inlet with packing tape, the cured parts were coated with clear acrylic spray (Krylon) and then dried in air to improve optical transparency. Finally, a small magnet was inserted into a hole located in the middle portion of the top piece (Figure S4a). Both pieces of the 3D printed housing were submerged in a SuperBlock buffer solution for 2 h prior to detection experiments to minimize non-specific adsorption of assay components with the polyester-based 3D-printed material.
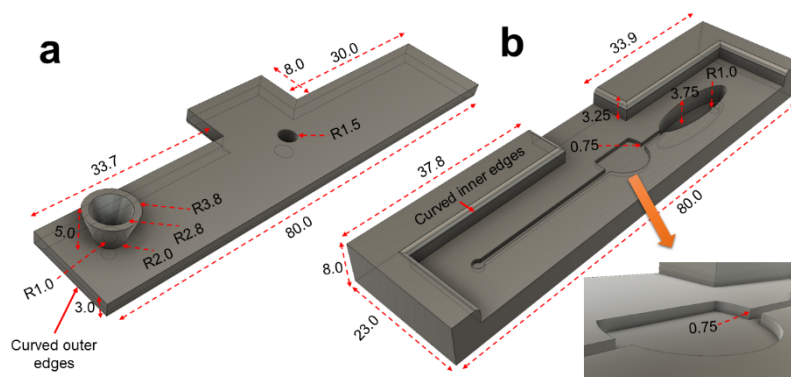

Figure S4. Autodesk Fusion 360 3D drawing of the 3D-printed housing of the *hy*Flow device. (a) top/ceiling piece and (b) bottom/floor piece of the *hy*Flow microfluidic chip. The inset shows an expanded view of the electrochemical detection zone. The contact points on the edges of both parts have mating curved shapes to ensure a firm fit. (all dimensions are given in mm, R = radius)

The *hy*Flow device was assembled as follows. First, the paper electrode was placed on the bottom piece of the 3D-printed chip with the features corresponding to the fluidic channel, outlet reservoir, and electrochemical detection zone on the paper aligned with the corresponding features in the chip (Scheme 1b, main text). Second, the top piece was added and aligned with the bottom piece. This resulted in the paper electrode being sandwiched between the top and bottom 3D-printed pieces (Figure S5).
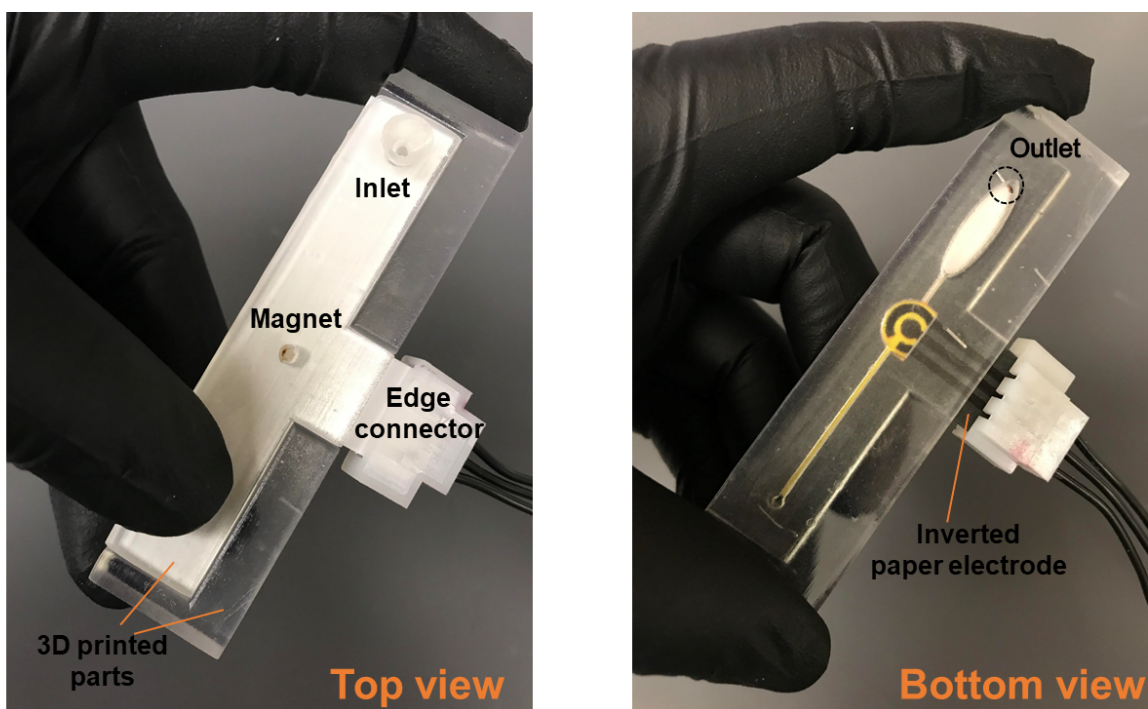

Figure S5. Photographs of the completed *hy*Flow device. The magnet in the top 3D printed piece is centered behind the working electrode to concentrate the MB-AgNP conjugates.

Edge connector. The housing for the edge connector (Headers & Wire Housings 3.96 mm Crimp Hsg F 3Ckt W/O Pos Lck, model number–538–172159–0003), crimp terminals (Headers & Wire Housings Crimp Term 18–20 Tin Brass Loose Pc, model number–538–172160–1806–LP), and Cu wires were purchased from Mouser Electronics (Mansfield, TX). Edge connectors were assembled by connecting crimp terminals with copper wires and inserting three of them into an edge connector housing. These connectors enable ohmic contact between the carbon electrodes (*hy*Flow or *no*Flow) and the potentiostat. In addition, the bottom piece of the edge connector used in the *no*Flow device incorporates a 3D-printed plastic extension containing a magnet aligned with the working electrode (WE). This is necessary to concentrate the MB–AgNP magnetic conjugates onto the WE (Figure S3b).

Preparation of MB-AgNP conjugates. To form the stock MB-AgNP conjugate, 100.0 µL of AgNP-bDNA (~6.0 x 10^{11} AgNPs/mL) was mixed with 16.0 µL of streptavidin-coated, 1.0 μm-diameter MBs (~7-10 x 10^9 MB/mL), and the suspension was shaken on a Bioshake iQ (Q Instruments, Jena, Germany) at 1400 rpm for 30 min at 25 ^{o}C in siliconized, low-retention microcentrifuge tubes.

Following conjugation, the MB-AgNP conjugates were rinsed three times by holding the microcentrifuge tube up to a magnet for 30 s, removing the supernatant, and resuspending the conjugates in 16.0 µL of BCl or BCl solutions containing sugar [(BCLS(2%), BCLS(10%), BCLS(20%),and BCLS(50%)]. In Figure S6, these are denoted as the 'stock in BCl' and the 'stock in BCLS(0-50%)' suspensions, respectively. In these stock suspensions, each MB hosts an average of 441 AgNPs. One or two microliters of the aforementioned stock suspensions were diluted to 50.0 µL (with either BCl or BClS(20%)) to yield the MB-AgNP conjugate samples used for specific experiments. The samples prepared using 1.0 μl and 2.0 μl of the stock suspension had AgNP concentrations of 125 pM and 249 pM, respectively (Figure S6, Sample-0,1,2 and Sample Set-3).Preparation of Sample-0 was identical to Sample-1, but they were used in two different experiments (see Table 1, main text). Sample set-4 represents the undiluted 'stock in BCLS(0-50%)' solutions, which were directly dried on the paper devices to perform the 'dry' assay.

A second set of stock MB-AgNP conjugates was prepared by mixing 16.0 µL of streptavidin-coated, 1.0 μm-diameter MBs with different concentrations of 100.0 µL Ag-bDNA solutions (Table S1) and resuspending in BClS(20%) to generate calibration plots for the 'dry' and 'wet' assays [denoted as Sample set-5 and Sample set-6 in Table 1(main text) and Figure S6].
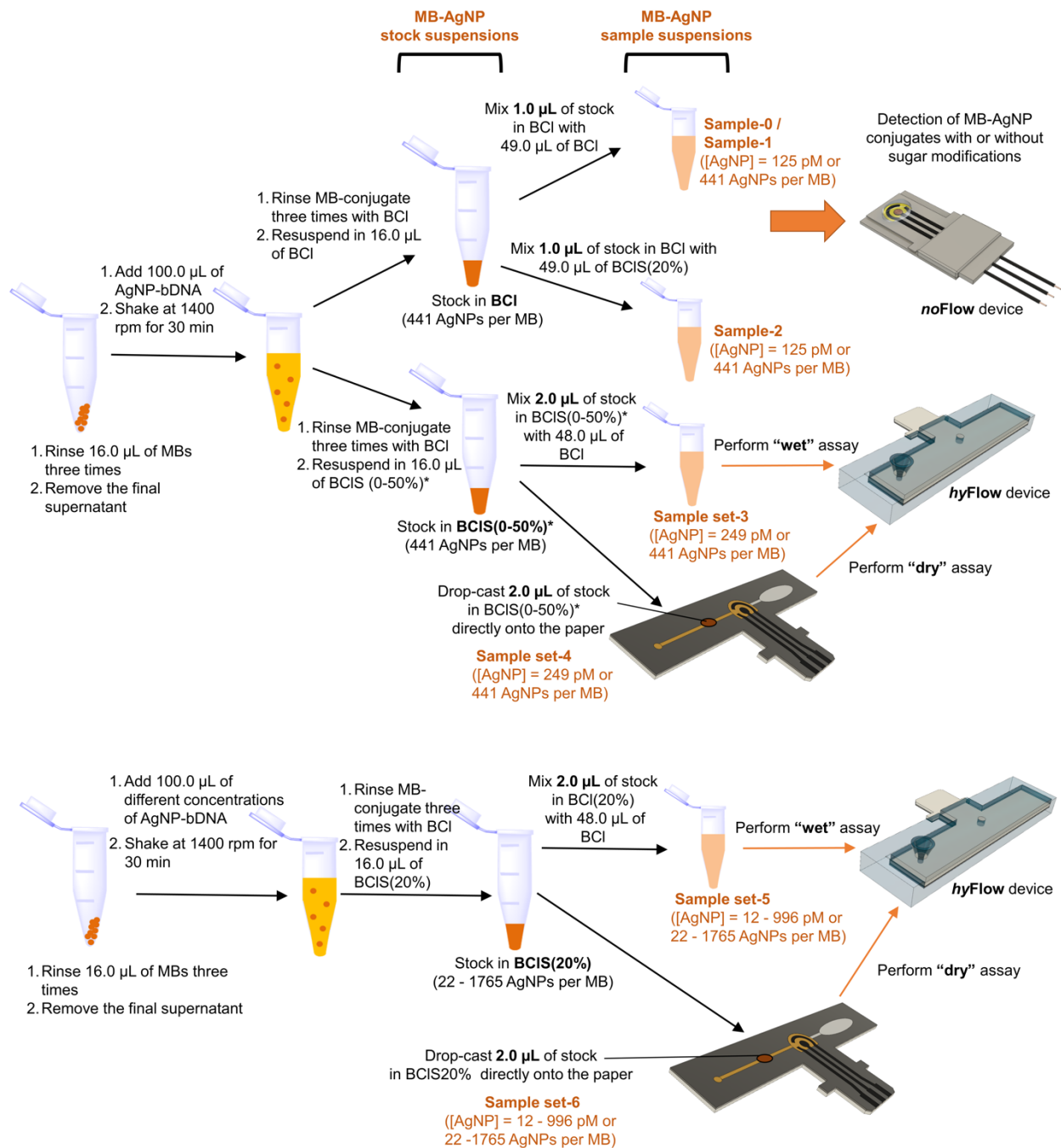
Figure S6. A flow chart showing the preparation of the MB–AgNP conjugates (stock and sample suspensions) in different BCl media, and subsequent detection using the *no*Flow and *hy*Flow devices.

Table S1. Characteristics of the MB–AgNP conjugates prepared to generate dose-response curves for the 'wet' and 'dry' assays [These data are also presented in Table 1 (main text) and Figure S6 as Sample sets 5 and 6].

MB–AgNP conjugate	Volume of Ag–bDNA solution (μL)[a]	Number of AgNPs[b]	Estimated AgNPs:MB ratio[c]	[AgNP] (pM) in 50 μL of sample[d]
1	5	3.00E+09	22	12
2	10	6.00E+09	44	25
3	25	1.50E+10	110	62
4	50	3.00E+10	221	125
5	100	6.00E+10	441	249
6	200	1.20E+11	882	498
7	400	2.40E+11	1765	996

(a) Volumes of AgNP–Biotin solution (~6.0 x 10^{11} AgNPs/mL) diluted or concentrated to 100.0 μL and then added to 16.0 μL of MBs.

(b) Total number of AgNPs available in the mixture to bind with the MB via streptavidin-biotin interaction.

(c) Average number of AgNP per MB.

(d) Concentration of AgNPs in the 50.0 μL of sample inserted into the *hy*Flow device for the 'wet' assay. In the 'dry' assay, the sample is not added to the inlet of the *hy*Flow device. Rather, it is drop-cast onto the paper electrode strip and subsequently resolvated prior to analysis. However, similar AgNP concentrations (as in 'wet' assay) were presented for the 'dry assay' conjugates by assuming that the drop-cast sample would resolvate inside the *hy*Flow device in a hypothetical volume of 50.0 μL during the resolvation step.

UV-vis characterization of MB-AgNP conjugate formation. Figure
S-7 shows UV-vis spectra of three different concentrations of
AgNP-bDNA solutions (corresponding to AgNP:MB ratios of 110, 441
and 1765, Table S1) before and after incubation with
streptavidin-coated MBs. Prior to addition of the MBs, two peaks
are present: one at 400 nm, which arises from the plasmon
excitation of individual AgNPs, and one at 260 nm, which
corresponds to the DNA coating on the AgNPs. After conjugation,
both peaks are absent from the spectra of the supernatant,
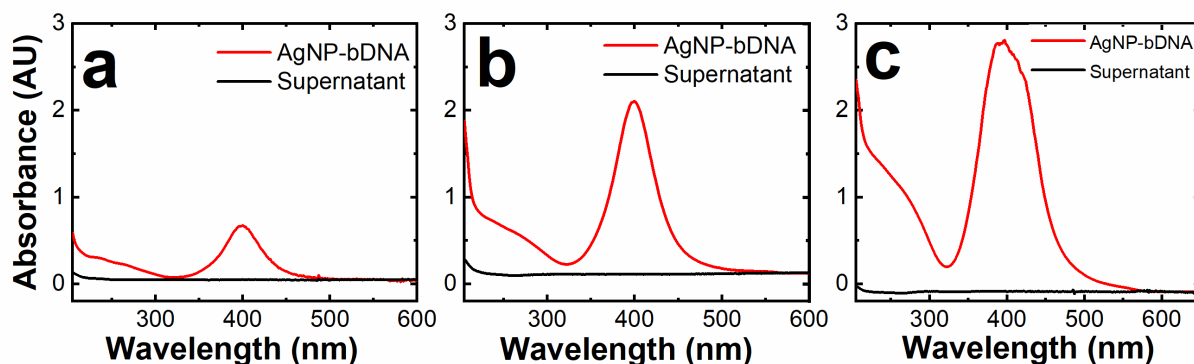indicating complete attachment of the AgNPs to the MμBs.

Figure S7. UV-vis spectra of the AgNP-biotin solution before
incubation with streptavidin-coated MBs (red trace) and the
supernatant after removal of the MBs (black trace) for the
formation of conjugates corresponding to AgNP:MB ratios of (a)
110, (b) 441, and (c) 1765.

Contact angle measurements of different colored wax. Different wax colors exhibit different degrees of hydrophobicity and, hence, affect pressure driven flow differently. Water contact-angle measurements showed that the yellow waxed areas are less hydrophobic (contact angle: $111^0 \pm 1^0$) compared to black waxed areas ($128^0 \pm 1^0$) (Figure S8). Consequently, there is better wettability on the yellow waxed areas compared to the black waxed areas on the paper electrodes. Therefore, the sample flow path and the electrochemical detection zone of the paper electrodes were fabricated with yellow wax.
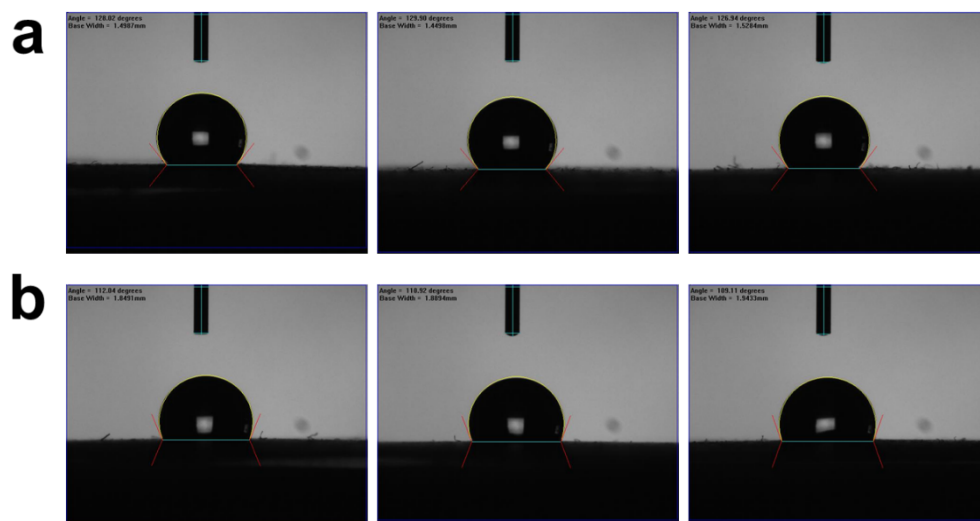

Figure S8. Contact angle measurements on different colored wax. The wax was printed, as described in the Experimental Section of the main text. Triplicate measurements are shown for (a) black wax areas and (b) yellow wax areas of the *hy*Flow paper electrodes.
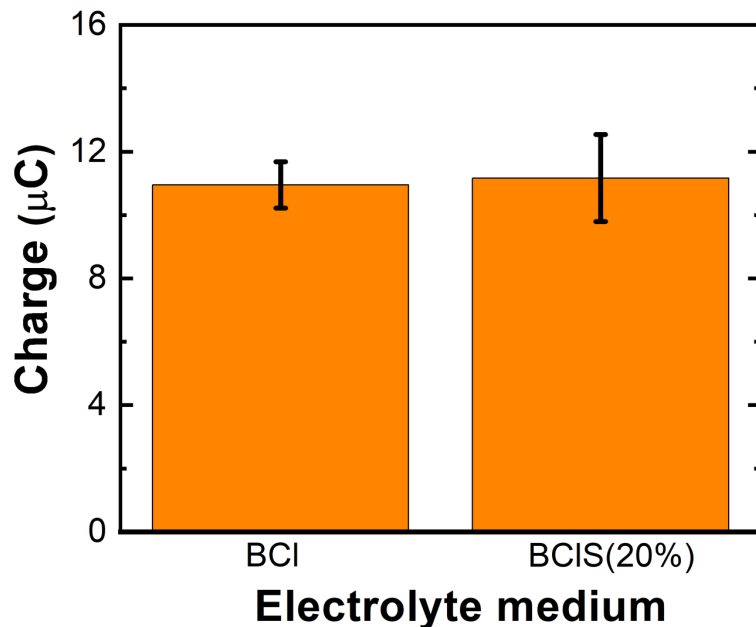
Figure S9. Histograms showing the average Ag charge (N=5) determined for detection of MB–AgNP conjugate samples prepared in BCl (Figure S6: Sample 0) and BClS(20%)(Figure S6: Sample 2).
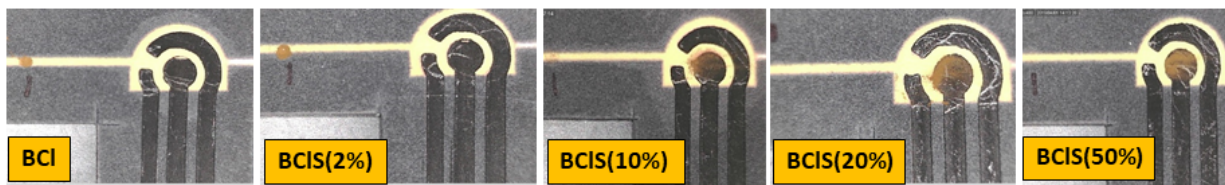

Figure S10. Photographs of paper electrodes after performing the 'dry' assay by drop-casting MB–AgNP stock conjugates on *hy*Flow devices. In this experiment, MB–AgNP stock conjugates were prepared in BCl, BClS(2%), BClS(10%), BClS(20%), BClS(50%). The brown patches located on the working electrode reveal the final locations of the MB–AgNP conjugates.

Comparison of assay performance as a function of the size of the magnetic beads. The 'wet' and 'dry' assays were tested using different sizes of magnetic particles to determine the optimal size. These magnetic particles were purchased from two different vendors and they have different characteristics: Streptavidin-coated, 1.0 μm-diameter MBs (binding capacity: 1100-1700 pmol/mg of free biotin, 10 mg/mL); 2.8 μm-diameter MBs (binding capacity: 650-900 pmol/mg of free biotin, 10 mg/mL); 227 nm-diameter magnetic nanoparticles (binding capacity: 4475 pmol/mg of free biotin, 5 mg/mL). Because the mass concentration of the 1.0 μm- and 2.8 μm-diameter MBs is twice as high as the 227 nm-diameter magnetic nanoparticles, we slightly modify the conjugation procedure to yield stock solutions of MB-AgNP conjugates having similar masses of MBs. The stock conjugates formed using the 1.0 μm and 2.8 μm microbeads followed the standard protocol illustrated in Figure S6, but the stock conjugate solution for the 227 nm-microbeads was formed using 32.0 μL of magnetic nanoparticles. Because all three types of MB-AgNP conjugate solutions contain the same mass of magnetic particles, the GE/ASV signals can be normalized by the biotin binding capacity. Normalized Ag charges are shown in Figure S11a. This result indicates that micron scaled beads generate significantly larger charge per binding event.

We have also noticed that a significant quantity of the 227 nM MB-AgNP conjugates stuck onto the paper device even after two washing steps performed during the 'dry' assay protocol (Figure S11b). This could be due to larger numbers of magnetic nanoparticles penetrating into deeper pores of the cellulose fiber network during the drying process.
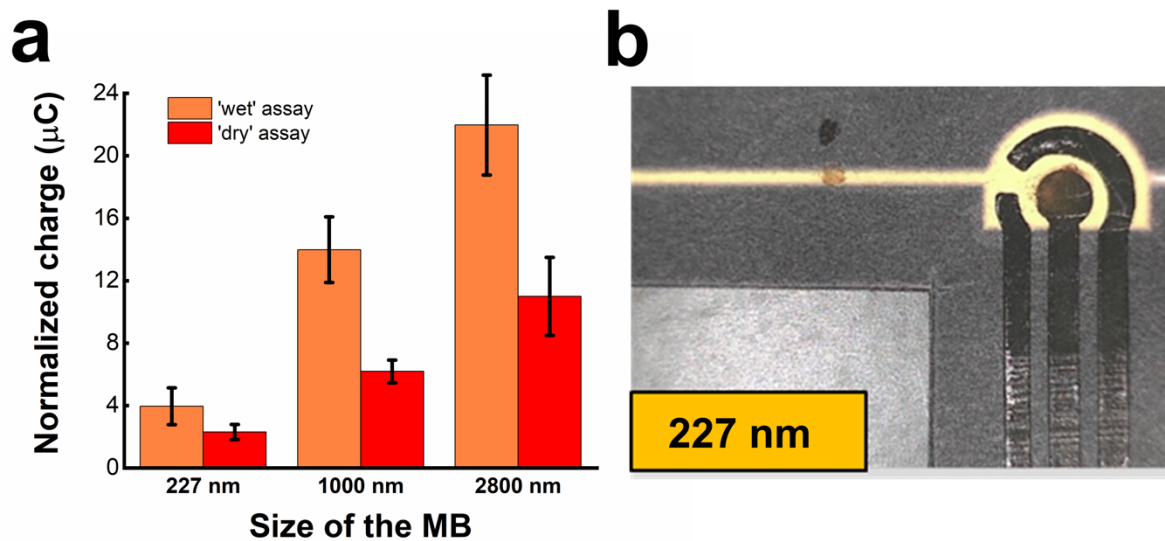
Figure S11. (a) Histogram showing the average Ag charge determined for the standard 'wet' (N=5) and 'dry' (N=5) assays using MB-AgNP conjugates prepared with three different sizes of magnetic particles. (b)Photograph of a paper electrode after performing the 'dry' assay by drop-casting 227 nm diameter MB-AgNP conjugates.

Hypothesis testing for the lower GE/ASV signals detected for the 'dry' assay. Aggregation of the MB–AgNP conjugates should result in lower GE/ASV charge compared to the 'wet' assay, regardless of how they resolvate into the solution. This can be confirmed by physically resolvating a pre-dried sample of MB–AgNP conjugates, and then quantifying the extent of resolvation using the 'wet' assay protocol. This hypothesis was tested using the following approach. First, 2.0 μL of MB–AgNP conjugate samples (Figure S6: Sample set-6, AgNP:MB = ~441) were drop-cast separately into a microcentrifuge tube and onto the sample flow path of a *hy*Flow paper electrode. The conjugates were then dried overnight under ambient laboratory conditions. Next, the conjugates were hydrated and resolvated with 50.0 μL BCl by pipette-mixing, and then they were collected into two separate microcentrifuge tubes. (Figure S12)
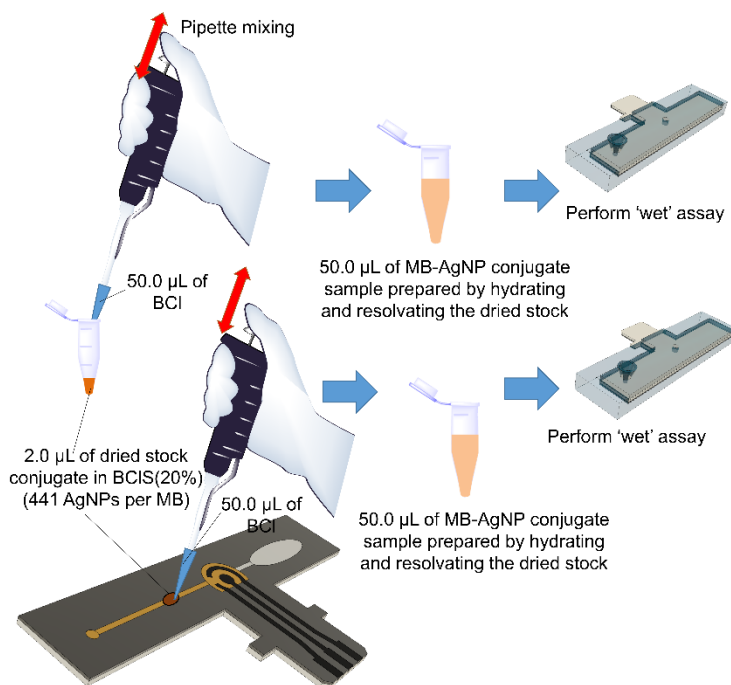

Figure S12. Resolvation of pre-dried MB–AgNP conjugates.

Finally, these MB–AgNP conjugates were detected by GE/ASV using the 'wet' assay protocol. Another 'wet' assay experiment was performed using a 50.0 μL MB–AgNP conjugate sample prepared from the same stock (but without drying) as a positive control. The two experiments resulted in 100% Ag signal recovery compared to the positive control (Figure S13). Therefore, we rejected the aggregation hypothesis.
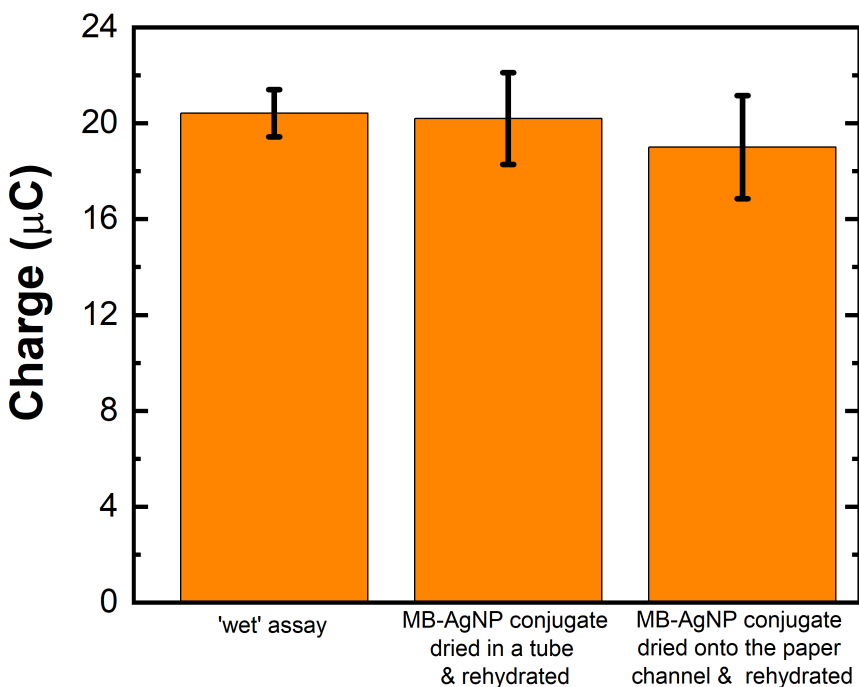

Figure S13. Histogram showing the average Ag charge determined for the typical 'wet' assay (N=3) and two different control assays (N=3) corresponding to the AgNP concentration of 249 pM or AgNP:MB ratio of 441 AgNP:MB (the stock conjugate is prepared in BClS(20%)).

We next assessed the hypothesis that the MB–AgNP conjugates are entrapped or otherwise nonspecifically adsorbed onto the 3D-printed chip or the paper electrode. We were unable to visually detect entrapment of conjugates inside the *hy*Flow device after

two washing steps. This can be confirmed by the real-time video recorded during the 'dry' assay (Movie S2). However, we suspect that only a small fraction of the conjugates remains stuck after successive hydration and washing steps. Therefore, conjugate entrapment is unlikely to be responsible for the observed ~55% signal loss observed for the 'dry' assay vs. to the 'wet' assay.

Finally, we inspected the distribution of MB-AgNP conjugates on the WE after performing the 'wet' and 'dry' assays. The results showed that the distribution of MB-AgNP conjugates on the *hy*Flow WE is different for the two assays (Figure S14). We believe this difference is likely responsible for most of the observed lowering of the ASV signal for the 'dry assay'.
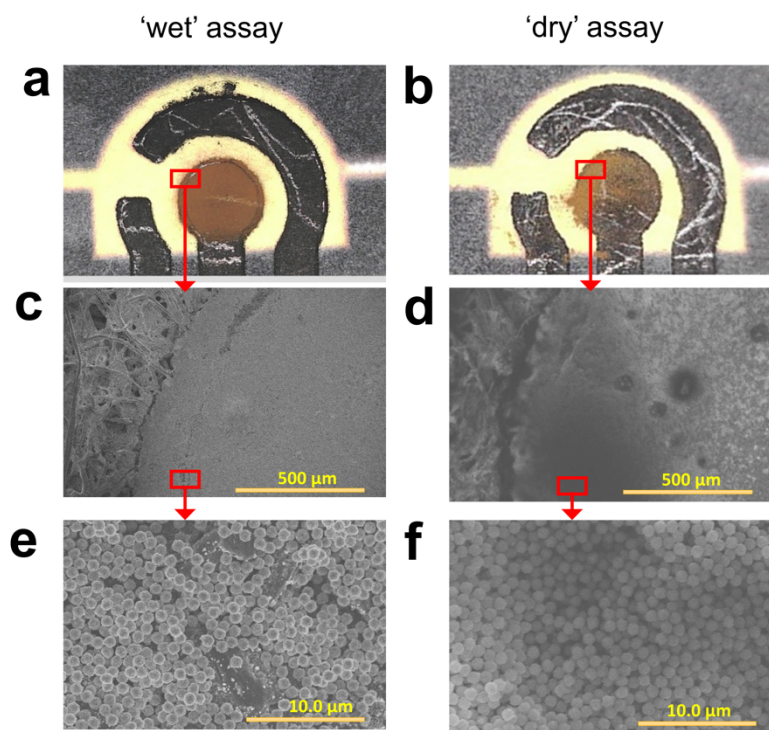

Figure S14. Photographs of paper electrodes after performing the (a) 'wet' and (b) 'dry' assays on *hy*Flow devices (Figure S6: Sample set-5 and Sample set-6; AgNP concentration = ~249 pM or AgNP:MB = ~441).SEM micrographs of MB-AgNP conjugates imaged on the carbon/Au working electrode after performing the GE/ASV detection for the (c and e) 'wet' and (d and f) 'dry' assays.

Table S2. Summary of results from prior studies in which hollow-channel paper analytical devices were used to detect micron-scale conjugates.

Conjugate type	diameter of the MB (μm)	Max Ag Charge detected (μC)	Ref.
MB–AgNP	2.8	~3.5	1
MB–Ricin–AgNP	2.8	~1.2	2
MB–AgNP	2.8	~7.5	3
MB–TFF3–AgNP	2.8	~4.0	4
MB–NTproBNP–AgNP	2.8	~1.2	5
MB–AgNP	1.0	26 ± 3.4	This work

Ricin =biological warfare agent

TFF3 = Trefoil Factor 3 (kidney disease marker)

NTproBNP = heart failure biomarker

Testing of the 'instant mix-1' assay with a larger amount of MBs. A modified 'instant mix-1' experiment was performed to determine the effect of the amount of MBs on the final GE/ASV signal. Specifically, 4.0 μL of MBs (~7–10 x 10^9 MB/mL) in BClS(20%) solution were drop-cast onto the yellow wax channel of the paper electrode in the two different configurations shown in Figure S15a. Next, the MB–AgNP conjugate was formed on-chip by injecting 100.0 μL of a AgNP-bDNA/DI water solution (~6.0 x 10^{11} AgNPs/mL) into the chip to hydrate the dried MBs. This was followed by a 2 min incubation step, two washing steps (each using 100.0 μL of BCl solution), and finally GE/ASV detection. The results revealed a GE/ASV charge of 6.0 ± 1.9 μC for the *Type i* deposition and 7.7 ± 1.9 μC for the *Type ii* deposition (Figure S15). These values are comparable to the Ag charge collected for the "instant mix-1 assay" (7.3 ± 1.9 μC) described in the main text, which utilized only 2.0 *μ*L of predried MBs. Accordingly, we conclude that 2.0 *μ*L of MBs is the optimized volume to use in the *hy*Flow device.
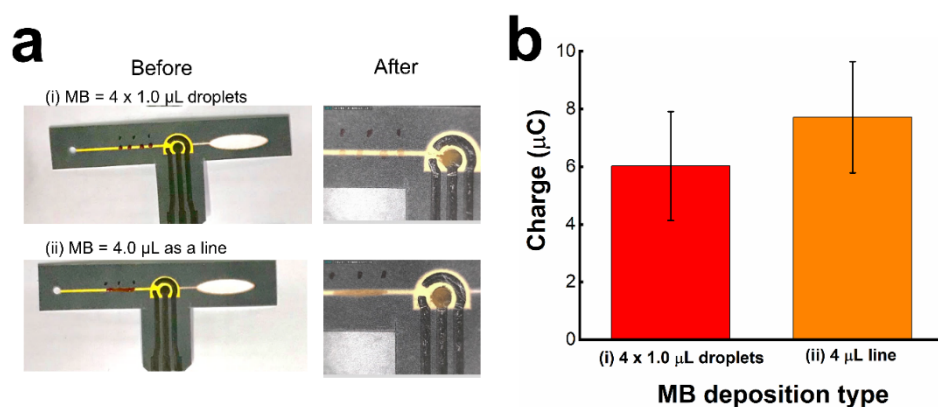

Figure S15. (a)Photographs of paper electrodes before and after performing the 'instant mix-1' assay using 4.0 *μ*L of pre-dried MBs (*Type i*) pre-dried as either four individual 1.0 *μ*L droplets or (*Type ii*) as a single 4.0 *μ*L-long line. (b) Histogram showing the GE/ASV charge determined for the *Type i* and *Type ii* experiments. The error bars represent the standard deviations for five measurements made using independently fabricated paper electrodes.

Movie S1. Video recorded during the 'wet' assay. The pre-formed MB–AgNP conjugate is pipetted into the inlet of the device and transported towards the electrode prior to the GE/ASV analysis.

Movie S2. Video recorded during the 'dry' assay. Pre-dried MB–AgNP conjugate is resolvated and transported towards the electrode prior to the GE/ASV analysis.

Movie S3. Video recorded during the 'instant mix — 2' assay. Resolvation, passive mixing and transportation of the predried MBs and AgNP-bDNA towards the electrode prior to the GE/ASV analysis.

References

1. K. Scida, J. C. Cunningham, C. Renault, I. Richards and R. M. Crooks, Anal. Chem., 2014, 86, 6501–6507.

2. J. C. Cunningham, K. Scida, M. R. Kogan, B. Wang, A. D. Ellington and R. M. Crooks, Lab on a chip, 2015, 15, 3707–3715.

3. J. C. Cunningham, M. R. Kogan, Y.-J. Tsai, L. Luo, I. Richards and R. M. Crooks, ACS Sensors, 2016, 1, 40–47.

4. P. R. DeGregory, Y.-J. Tsai, K. Scida, I. Richards and R. M. Crooks, The Analyst, 2016, 141, 1734–1744.

5. P. R. DeGregory, J. Tapia, T. Wong, J. Villa, I. Richards and R. M. Crooks, IEEE J Transl Eng Health Med, 2017, 5, 1-6